Magnetic Studies on Eu_3MO_7 (M = Nb, Ta, Ir) with Fluorite-related Structure by ^{151}Eu Mössbauer Spectroscopy and Magnetic Susceptibility Measurements

Yukio Hinatsu, Yoshihiro Doi and Makoto Wakeshima

Division of Chemistry, Hokkaido University, Sapporo 060-0810, Japan

Keywords: Magnetic properties; Europium; Mössbauer spectrum; Magnetic susceptibility

Abstract

Magnetic properties of europium-containing compounds Eu_3MO_7 (M = Nb, Ta, Ir) with fluorite-related structure have been investigated. Magnetic susceptibility measurements show that all these compounds are paramagnetic and have no magnetic ordering down to 1.8 K. At very low temperatures (T < 50 K), the susceptibilities of each compound attain constant values, which is characteristic of the ground state for Eu^{3+} ions. The results of ^{151}Eu Mössbauer spectroscopic measurements show that the asymmetric parameter for Eu(2) in seven-coordination is much larger than that for Eu(1) in cubic environment, which in accordance with the crystallographic result.

1. Introduction

Recently, the rare-earth transition metal oxides with general composition Ln_3MO_7 (*Ln* = rare earths; *M* = transition metals such as Nb, Ru, Ta et al.) have been widely investigated from the viewpoint of their one-dimensional nature. They have a defect-fluorite structure. The relationship to the fluorite structure is as follows. The fluorite unit cell for oxides has the composition $M^{4+}{}_4O_8$. If the four tetravalent metal ions are replaced by three trivalent ions (*Ln*) and one pentavalent ion (*M*), one oxide vacancy is formed per fluorite cell. Due to the significant differences in radii between the Ln^{3+} and M^{5+} ions, cation ordering occurs on the metal sites and the oxide-vacancy orders on the anion sites. The M^{5+} ion is coordinated with six oxygen ions, forming an MO_6 octahedron. These octahedra share corners forming one-dimensional chains which are oriented along the *c*-axis [1-7].

Many studies have been performed [8-37], due to this unique crystal structure and possible related magnetic properties for Ln_3MO_7 compounds (*M* = Mo, Ru, Re, Os, Ir), especially for the magnetic properties of compounds containing Ru^{5+} ion at the *M*-site because of its largest possible spin ($S = 3/2$) among the 4*d* and 5*d* transition metals. However, there was scant evidence for the expected one-dimensionality in the magnetic susceptibility.

This type of compound Ln_3MO_7 is also attractive because it exhibits dielectric properties [38, 39] as well as photocatalytic activity [40, 41].

In the case that *M* ions are diamagnetic, magnetic properties of Ln_3MO_7 are due to magnetic interactions between *Ln* ions. There are two kinds of oxygen-coordination environment around *Ln* ions. One-third of the *Ln* ions are coordinated by eight oxygen ions and the remaining two-third of the *Ln* ions are seven-coordinated. Previous magnetic susceptibility and specific heat measurements on Ln_3MO_7 (*Ln* = Nd, Tb; *M* = Nb, Sb, Ta) showed “two-step” magnetic transition [30, 42-44]. It is discussed that the eight-coordinate *Ln* (1) and seven-coordinate *Ln* (2) ions individually order at different temperatures.

In order to elucidate the role of each *Ln*(1) and *Ln*(2) ions on the magnetic properties of Ln_3MO_7 compounds, we prepared europium containing compounds Eu_3MO_7 (*M* = Nb, Ta, Ir). Through X-ray diffraction measurements, their structures were determined, and magnetic susceptibility and ^{151}Eu Mössbauer Spectroscopy measurements were performed to study their magnetic properties.

2. Experimental

2.1. Sample preparation

Polycrystalline samples of Eu_3MO_7 (*M* = Nb, Ta, Ir) were prepared by the standard solid-state reaction. Europium sesqui-oxides Eu_2O_3, niobium oxides Nb_2O_5, tantalum oxides Ta_2O_5, and Ir metals were used as starting materials. These starting materials were well mixed in an agate mortar. The mixtures were pressed into pellets, and heated in the following conditions. For preparing Eu_3NbO_7 and Eu_3TaO_7, the pellets were heated in air at 1300 and 1500 °C, respectively for 12 h. Eu_3IrO_7 were prepared in flowing oxygen atmosphere at 1200 °C for 12h. These heating procedure were repeated twice. In the first stage of sample preparations, very small amounts of impurities remained in the desired compounds; they were unreacted starting materials Eu_2O_3. In order to remove these impurities, the samples were washed with diluted hydrochloric acid. After this treatment, single-phase Eu_3MO_7 (*M* = Nb, Ta, Ir) compounds could be obtained.

2.2. X-ray diffraction measurements

Powder X-ray diffraction profiles were measured using a Rigaku Multi-Flex diffractometer with Cu-Kα radiation equipped with a curved graphite monochromator. The data were collected by step-scanning in the angle range of $10° \leq 2\theta \leq 120°$ at a 2θ step-size of 0.02°. The X-ray diffraction data were analyzed by the Rietveld technique, using the program RIETAN-FP [45] and the crystal structure was drawn by VESTA program [46].

2.3. Magnetic susceptibility measurements

The temperature-dependence of the magnetic susceptibility was measured in an applied field of 0.1 T over the temperature range of 1.8 K ≤ T ≤ 400 K, using a SQUID magnetometer (Quantum Design, MPMS5S). The susceptibility measurements were performed under both zero-field-cooled (ZFC) and field-cooled (FC) conditions. The former was measured upon heating the sample to 400 K under the applied magnetic field of 0.1 T after zero-field cooling to 1.8 K. The latter was measured upon cooling the sample from 400 to 1.8 K in the applied field of 0.1 T.

2.4. ^{151}Eu Mössbauer spectroscopy measurements

The ^{151}Eu Mössbauer spectra were measured with a Mössbauer spectrometer VT-6000 (Laboratory Equipment Co.) in the constant acceleration mode using a radiation source $^{151}SmF_3$ (1.85 GBq). The spectrometer was calibrated with a spectrum of α-Fe at room temperature. The γ-rays were detected with a NaI scintillation counter. Europium trifluoride (EuF_3) was used as a reference standard for the chemical isomer shift. The sample was wrapped in an aluminum foil so as to have its average surface density of 10 mg (Eu) cm^{-2}.

3. Results and Discussion

3.1. Crystal structure

The X-ray diffraction patterns for Eu_3MO_7 (M = Nb, Ta, and Ir) are shown in Figs. 1 (a), (b), and (c), respectively, and they are similar to that for the fluorite structure. All reflections appeared to be consistent with the *C*-centered conditions, $h + k = 2n$, and $h\,0\,l$ reflections with odd l are absent.

We have analyzed the X-ray diffraction profiles Eu_3IrO_7 with the space group *Cmcm*, which is the most found one for the Ln_3MO_7 compounds, and all the reflections observed for Eu_3IrO_7 could be successfully indexed.

For the X-ray diffraction profiles for Eu_3NbO_7 and Eu_3TaO_7, there exist many very weak $h0l$ reflections with odd l, which could not be indexed based on the *Cmcm*. We analyzed the

X-ray diffraction profiles for Eu_3NbO_7 and Eu_3TaO_7 with the space group $C222_1$. The space group $C222_1$ is the subgroup of *Cmcm*, and found for some Ln_3MO_7-type compounds with medium sized rare earths [1, 30, 42]. All the reflections observed could be successfully indexed. The refinement by using the structural model with the space group $C222_1$ converged rapidly, and yielded low residual factors and acceptably low values for the calculated standard deviations of refined parameters. Table 1 lists the lattice parameters and atomic coordinates for Eu_3MO_7 (*M* = Nb, Ta, Ir). Figures 2 (a) and (b) illustrate the crystal structures of Eu_3NbO_7 (Space group: $C222_1$) and Eu_3IrO_7 (*Cmcm*), respectively. Both the structures have similar features: two kinds of infinite chains formed by corner-sharing NbO_6 (IrO_6) octahedra and edge-sharing $Eu(1)O_8$ cubes, the slabs consisting of alternate chains, and 7-coordinated Eu(2) ions exiting between the slabs. For these two structures, the NbO_6 (IrO_6) octahedron and $Eu(1)O_6$ cube in the *Cmcm* structure are obviously much more regular than those in the $C222_1$. In both the structures, the MO_6 octahedra running along the *c*-axis. They are tilted towards the 1 0 0 direction in the $C222_1$ structure, while in the *Cmcm* structure, they are tilted towards the 0 1 0 direction. Some selected bond lengths and angles for Eu_3MO_7 (*M* = Nb, Ta, Ir) are summarized in Table 2.

3.2. Magnetic properties

3.2.1. Magnetic susceptibility

Magnetic susceptibility measurements for Eu_3MO_7 (*M* = Nb, Ta, Ir) show that no magnetic coorperative phenomena have been observed down to 1.8 K and there is no divergence between ZFC and FC magnetic susceptibilities through experimental temperature range. Although the electronic structure of Ir^{5+} is $[Xe](4f)^{14}(5d)^4$ ([Xe] is the xenon core electron configuration), its magnetic behavior is known to be almost non-magnetic [47]. Since Nb^{5+} and Ta^{5+} are both diamagnetic, only Eu^{3+} ions contribute to the paramagnetic behavior of Eu_3MO_7 (*M* = Nb, Ta, Ir).

Figure 3 depicts the magnetic susceptibility vs. temperature curve for Eu_3MO_7 (M = Nb, Ta, Ir). The shape of the susceptibility vs. temperature curve is characteristic of Van Vleck

paramagnetism for Eu^{3+} [48], with a constant value at the lower temperature region and a decreasing susceptibility with increasing temperature when T > 50 K.

The ground state of Eu^{3+} ion is nonmagnetic ($^7F_0$), and the excited states ^7F_J (J = 1, 2, --) are close to give energy differences comparable to k_BT at room temperature. The molar magnetic susceptibility for Eu^{3+} taking into account the contribution from the excited state is given by the following equation [48]:

$$\chi_{Eu^{3+}} = \frac{N_A \mu_B{}^2 / 3k_B}{\gamma T} \frac{24 + (13.5\gamma - 1.5)e^{-\gamma} + (67.5\gamma - 2.5)e^{-3\gamma} + (189\gamma - 3.5)e^{-6\gamma} \cdots}{1 + 3e^{-\gamma} + 5e^{-3\gamma} + 7e^{-6\gamma} + \cdots} \quad (1)$$

where the parameter $\gamma = \lambda/k_BT$ is the ratio of the overall multiplet width to the thermal energy (k_BT) (λ : the spin-orbit coupling constant), and γ is 1/21 for the Eu^{3+} ion. By fitting Eq.(1) to the experimental magnetic susceptibility above 100 K, the value of λ for Eu_3NbO_7, Eu_3TaO_7, and Eu_3IrO_7 was obtained to be 214, 210, and 221 cm^{-1}, respectively. These values of λ are smaller than the values reported for double perovskites, for example, 364 cm^{-1} for Sr_2EuIrO_6 [49] and 339 cm^{-1} for Ba_2EuNbO_6 [50].

3.2.2. Mössbauer spectra

Figures 4 (a), (b), and (c) are the Mössbauer spectra for Eu_3NbO_7, Eu_3TaO_7, and Eu_3IrO_7, respectively, measured at room temperature in the velocity range of -10 mm/s < v < 10 mm/s. As the structural analysis has indicated that the Eu ions occupy two kinds of sites, we assume two different environments for europium ions in analyzing these spectra. The ratio of their sites is Eu(1) : Eu(2) = 1:2.

First, we will discuss the isomer shift (IS) determined in this study. The isomer shift δ is proportional to the difference in the probability density for the electrons at the nucleus of the absorber $\Psi_A(0)$ and the source $\Psi_S(0)$, and to the difference between the nuclear radii in the excited and the ground state ΔR, and it is given by

$$\delta \propto \{|\Psi_A(0)|^2 - |\Psi_S(0)|^2\} \times \Delta R \qquad (2)$$

In the case of europium, the sign of ΔR is positive. Therefore, the IS increases with increasing electron density at the nucleus of absorber (i.e., at the sample). As the Eu-O bond length is shorter, its stronger covalency weakens the shielding effect of the 4*f* electron on the 6*s* orbital. Therefore, a negative linear relationship between the IS of Eu^{3+} and the Eu-O bond length has been reported for various europium-containing oxides [51, 52]. In this experiment, the isomer shifts of Eu(1) and Eu(2) are determined to be 0.1 and 0.7 mm/s, respectively. Since the average bond length of Eu(1)-O (2.50~2.54 Å) is longer than that of Eu(2)-O (2.34~2.36 Å), the trend of the isomer shifts is in accordance with the above relationship. Since the Eu(1) and Eu(2) sites have the point symmetry 2/*m* and *m*, respectively for the *Cmcm* space group, an electric field gradient (EFG) tensor exists, i.e., we have to consider the effect of an electric quadruple coupling $eV_{zz}Q_g$ at their sites. The interaction between the EFG tensor and the electric quadruple moment Q_g is described by the following Hamiltonian,

$$H_Q = \frac{eV_{zz}Q_g}{4I(2I-1)}\left(3I_z^2 - I(I+1) + \eta(I_x^2 + I_y^2)\right) \qquad (3)$$

where I is the nuclear spin, η is the asymmetric parameter, and V_{ii} is the electronic field gradient tensor. The EFG tensor of principal direction, V_{zz}, is divided into two components; it is given by $V_{zz} = V_{lattice} + V_{4f}$, where $V_{lattice}$ is the component of the contribution of the lattice, i.e., the crystal field formed from the coordinated oxygen ions, and V_{4f} is the component of the contribution of the 4*f* orbitals of the europium ions. The asymmetry parameter η is given by $\eta = (V_{xx} - V_{yy}) / V_{zz}$. If the point symmetry of the europium site is lower than threefold symmetry (-3*m*), this parameter should be considered. The isomer shift (IS), the electric quadruple coupling ($eV_{zz}Q_g$), and the asymmetry parameter (η) determined for Eu_3MO_7 (M = Nb, Ta, Ir) are summarized in Table 3. Although some europium oxides containing distorted EuO_6 octahedra, such as monoclinic perovskites give positive quadruple coupling constants [49, 50], most of europium oxides have negative values. In this study, $eV_{zz}Q_g$ is negative for both the sites Eu(1) and Eu(2). The

asymmetric parameters η for Eu(1) and Eu(2) are determined to be 0.2 and 0.8, respectively. The asymmetric parameter for Eu(2) is much larger than that for Eu(1). This result is in accordance with the crystallographic result that the symmetry of the 7-coordinated site Eu(2) is lower than that of the 8-coordinated site Eu(1).

References

[1] H. J. Rossell, *J. Solid State Chem*., **27**, 115-122 (1979).

[2] F. P. F. van Berkel and D. J. W. IJdo, *Mater. Res. Bull*., **21**, 1103-1106 (1986).

[3] W. A. Groen, F. P. F. van Berkel, and D. J. W. IJdo, *Acta Crystallogr*. Sec. **C 43**, 2262-2264 (1986).

[4] A. Kahn-Harari, L. Mazerrolles, D. Michel, and F. Robert, *J. Solid State Chem*., **116**, 103-106 (1995).

[5] P. Khalifah, R. W. Erwin , J. W. Lynn, Q. Huang, B. Batlogg, and R. J. Cava, *Phys. Rev.*, **B 60**, 9573-9578 (1999).

[6] F. Wiss, N. P. Raju, A. S. Wills, and J. E. Greedan, *Inter. J. Inorg. Mater.*, **2**, 53-59 (2000).

[7] B. P. Bontchev, A. J. Jacobson, M. M. Gospodinov, V. Skumryev, V. N. Popov, B. Lorenz, R. L. Meng, A. P. Litvinchuk, M. N. Iliev, *Phys. Rev.*, **B 62**, 12235-12240 (2000).

[8] D. Harada and Y. Hinatsu, *J. Solid State Chem*., **158**, 245-253 (2001).

[9] D. Harada, Y. Hinatsu, and Y. Ishii, *J. Phys.: Condens. Matter*, **13**, 10825-10836 (2001).

[10] D. Harada and Y. Hinatsu, *J. Solid State Chem*., **164**, 163-168 (2002).

[11] R. Lam, F. Wiss, and J. E. Greedan, *J. Solid State Chem.* **167**, 182-187 (2002).

[12] W. R. Gemmill, M. D. Smith, and H-C, zur Loye, *Inorg. Chem*., **43**, 4254-4261 (2004).

[13] R. Lam, T. Langet, and J. E. Greedan, *J. Solid State Chem.* **171**, 317-323 (2002).

[14] Y. Hinatsu, M. Wakeshima, N. Kawabuchi, and N. Taira, *J. Alloys Compd*., **374**, 79-83 (2004).

[15] M. Wakeshima and Y. Hinatsu, *J. Solid State Chem*., **179**, 3575-3581 (2006).

[16] J. R. Plaisier, R. J. Drost, and D. J. W. IJdo, *J. Solid State Chem.* **169**, 189-198 (2002).

[17] W. R. Gemmill, M. D. Smith, Y. A. Mozharivsky, G. J. Miller, and H-C, zur Loye, *Inorg. Chem.*, **44**, 7047-7055 (2005).

[18] Y. Hinatsu and Y. Doi, *J. Solid State Chem.*, **198**, 176-185 (2013).

[19] R. Morrow, M. A. Susner, M. D. Sumption, and P. M. Woodward, *Phys. Rev.*, **B 92**, 134402 (2015).

[20] H. Nishimine, M. Wakeshima, and Y. Hinatsu, *J. Solid State Chem*., **177**, 739-744 (2004).

[21] Y. Hinatsu, Y. Doi, H. Nishimine, M. Wakeshima, and M. Sato, *J. Alloys Compd*., **488**, 541-545 (2009).

[22] M. Wakeshima, D. Harada, and Y. Hinatsu, *J. Alloys Compd*., **287**, 130-136 (1999).

[23] J. E. Greedan, N. P. Raju, A. Wegner, P. Gougeon, and J. Padiou, *J. Solid State Chem.*, **129**, 320-327 (1997).

[24] H. Nishimine, M. Wakeshima, and Y. Hinatsu, *J. Solid State Chem.*, **178**, 1221-1229 (2005).

[25] Y. Doi, M. Wakeshima, and Y. Hinatsu, *J. Mater. Chem.*, **11**, 3135-3140 (2001).

[26] N. Ishizawa, K. Tateishi, S. Kondo, and T. Suwa, *Inorg. Chem*., **47**, 558-566 (2008).

[27] G. Wltschek, H. Paulus, I. Svoboda, H. Ehrenberg, and H. Fuess, *J.Solid State Chem*. **125**, 1-4 (1996).

[28] Y. Hinatsu and Y. Doi, *J. Solid State Chem.*, **220**, 22-27 (2014).

[29] J. F. Vente, R. B. Helmholdt, and D. J. W. IJdo, *J. Solid State Chem*. **108**, 18-23 (1994).

[30] M. Wakeshima, H. Nishimine, and Y. Hinatsu, *J. Phys.: Condens. Matter*, **16**, 4103-4120 (2004).

[31] J. F. Vente and D. J. W. IJdo, *Mater. Res. Bull.*, **26**, 1255-1262 (1991).

[32] M. Inabayashi, Y. Doi, M. Wakeshima and Y. Hinatsu, *J. Solid State Chem.*, **250**, 100-106 (2017).

[33] M. Inabayashi, Y. Doi, M. Wakeshima and Y. Hinatsu, *J. Solid State Chem.*, **254**, 150-154 (2017).

[34] Y. Hinatsu and Y. Doi, *J. Solid State Chem.*, **182**, 1694-1699 (2009).

[35] N. Barrier and P. Gougen, *Acta Crystallogr.*, **E59**, i22-i24 (2003).

[36] N. Barrier and P. Gougen, *Acta Crystallogr.*, **C63**, i102-i104 (2003).

[37] M. Wakeshima and Y. Hinatsu, *J. Solid State Chem.*, **183**, 2681-2688 (2010).

[38] L. Cai and J. C. Nino, *J. European Ceramic Soc.*, **27**, 3971-3976 (2007).

[39] L. Cai and J. C. Nino, *J. European Ceramic Soc.*, **30**, 307-313 (2010).

[40] R. Abe, M. Higashi, Z. G. Zou, K. Sayama, Y. Abe, and H. Arakawa, *J. Phys. Chem. B.*, **108**, 811-814 (2004).

[41] R. Abe, M. Higashi, K. Sayama, Y. Abe, and H. Sugihara, *J. Phys. Chem. B.*, **110**, 2219-2226 (2006).

[42] Y. Doi, Y. Harada, and Y. Hinatsu, *J. Solid State Chem.*, **182**, 709-715 (2009).

[43] Y. Hinatsu and Y. Doi, *J. Solid State Chem.*, **217**, 16-21 (2014).

[44] Y. Hinatsu and Y. Doi, *J. Solid State Chem.*, **239**, 214-219 (2016).

[45] F. Izumi and K. Momma, *Solid State Phenom.*, **130**, 15-20 (2007).

[46] K. Momma and F. Izumi, *Appl. Crystallogr.*, **41**, 653-658 (2008).

[47] M. Wakeshima, D. Harada, and Y. Hinatsu, *J. Alloys Compd.*, **287**, 130-136 (1999).

[48] J. H. Van Vleck, Theory of Electric and Magnetic Susceptibilities, Oxford, Clarendon, 1932.

[49] M. Wakeshima, D. Harada, and Y. Hinatsu, *J. Solid State Chem.*, **147**, 618-623 (1999).

[50] K.Henmi and Y. Hinatsu, *J. Solid State Chem.*, **148**, 353-360 (1999).

[51] S. Tanabe, K. Hirao and N. Soga, *J. Non-Cryst. Solids*, **113**, 178-184 (1989).

[52] A. Nakamura, N. Masaki and M. Saeki, *Ceram. Trans.*, **71**, 295-306 (1996).

Figure captions

Fig. 1. Powder x-ray diffraction patterns and Rietveld refinements for (a) Eu_3NbO_7, (b) Eu_3TaO_7, and (c) Eu_3TaO_7. The bottom trace is a plot of the difference between observed +(cross makers) and calculated (solid line) intensities. All allowed Bragg reflections are shown by vertical lines.

Fig. 2 Crystal structures of (a) Eu_3NbO_7 and Eu_3TaO_7 (space group: $C222_1$) and (b) Eu_3IrO_7 (*Cmcm*).

Fig. 3 Temperature dependence of magnetic susceptibility for (a) Eu_3NbO_7, (b) Eu_3TaO_7, and (c) Eu_3IrO_7 in the temperature range of 1.8 and 350 K. The solid line is calculated with Eq. (1) (see text).

Fig. 4 The ^{151}Eu Mössbauer spectra of (a) Eu_3NbO_7, (b) Eu_3TaO_7, and (c) Eu_3IrO_7. The red line is a calculated line with Lorentzian.

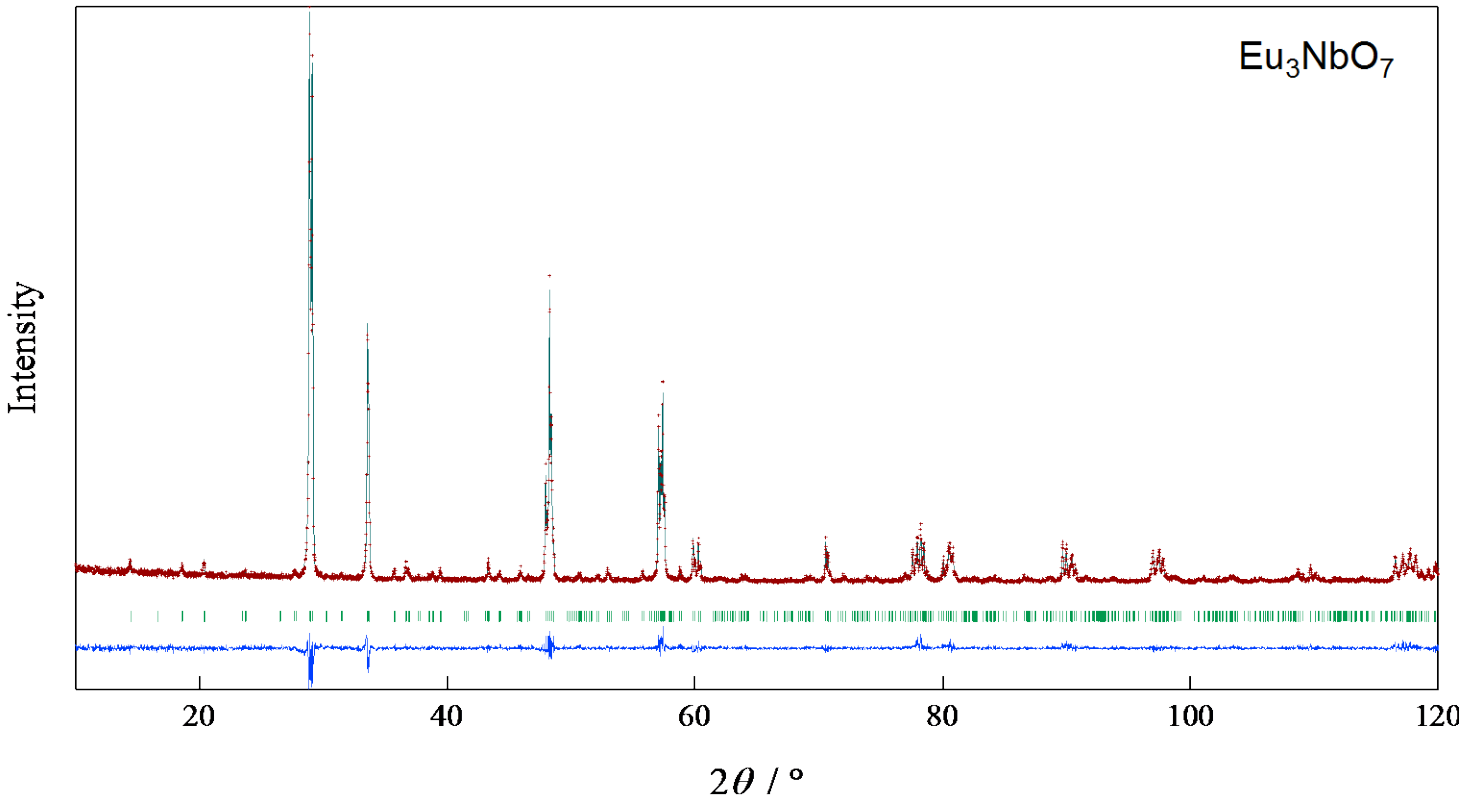

Fig.1(a)

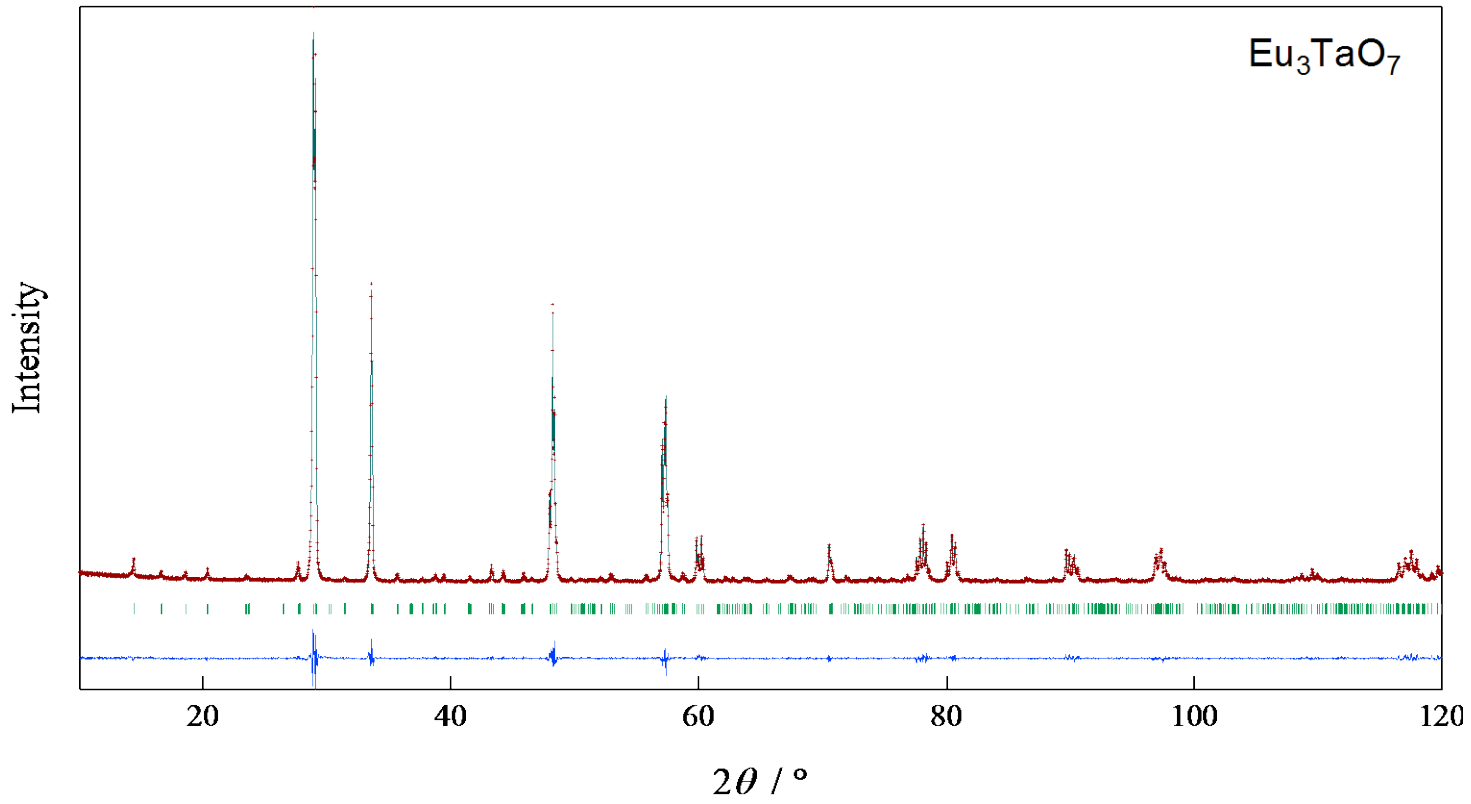

Fig.1(b)

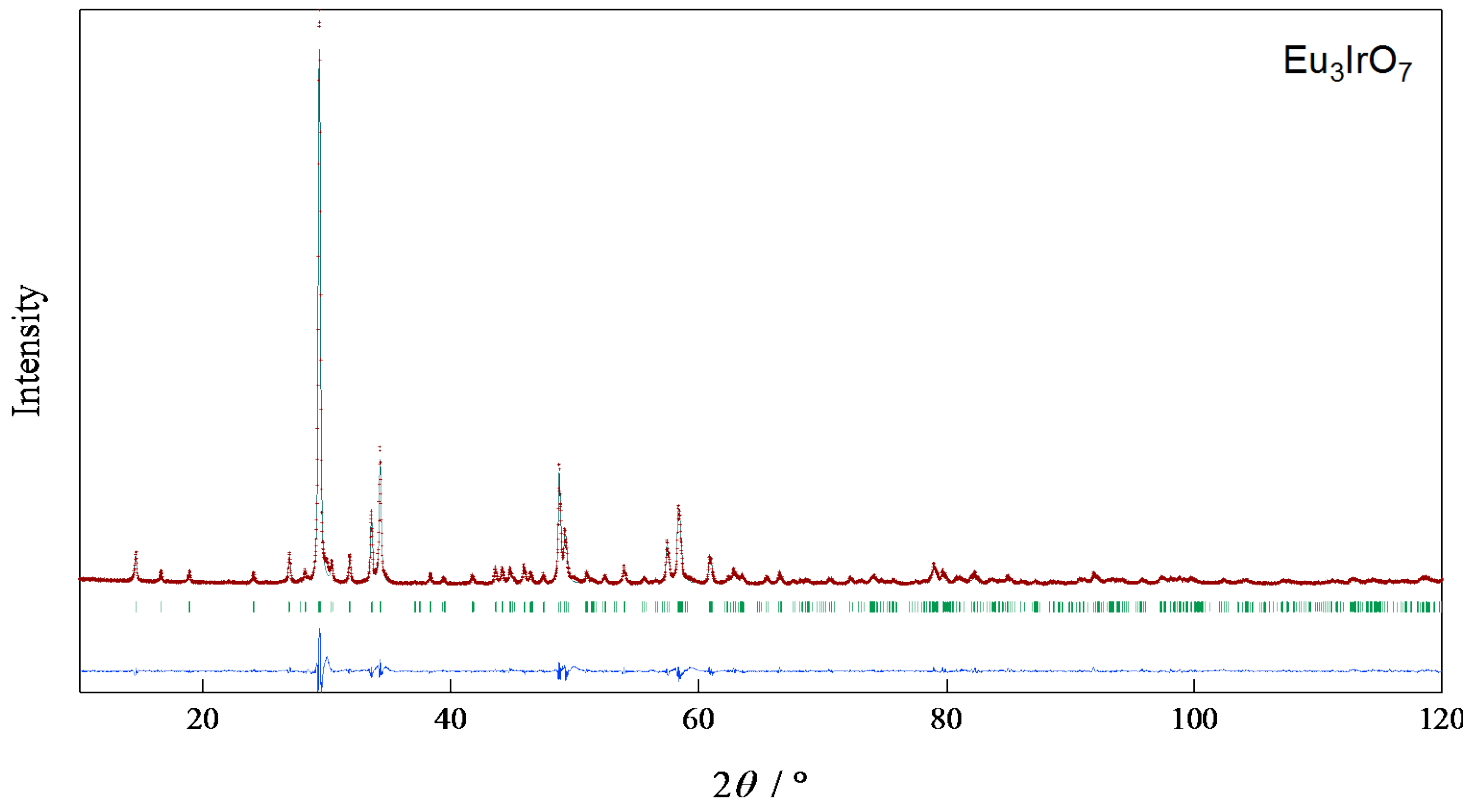

Fig.1(c)

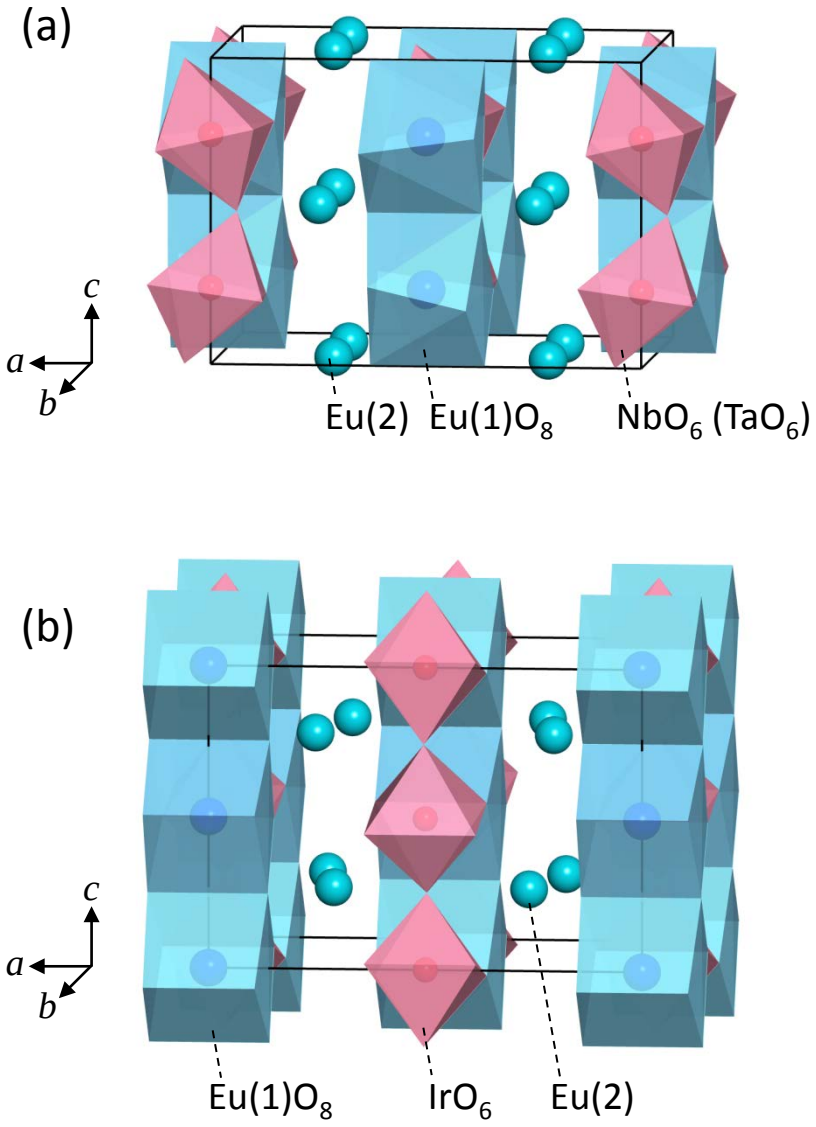

Fig.2

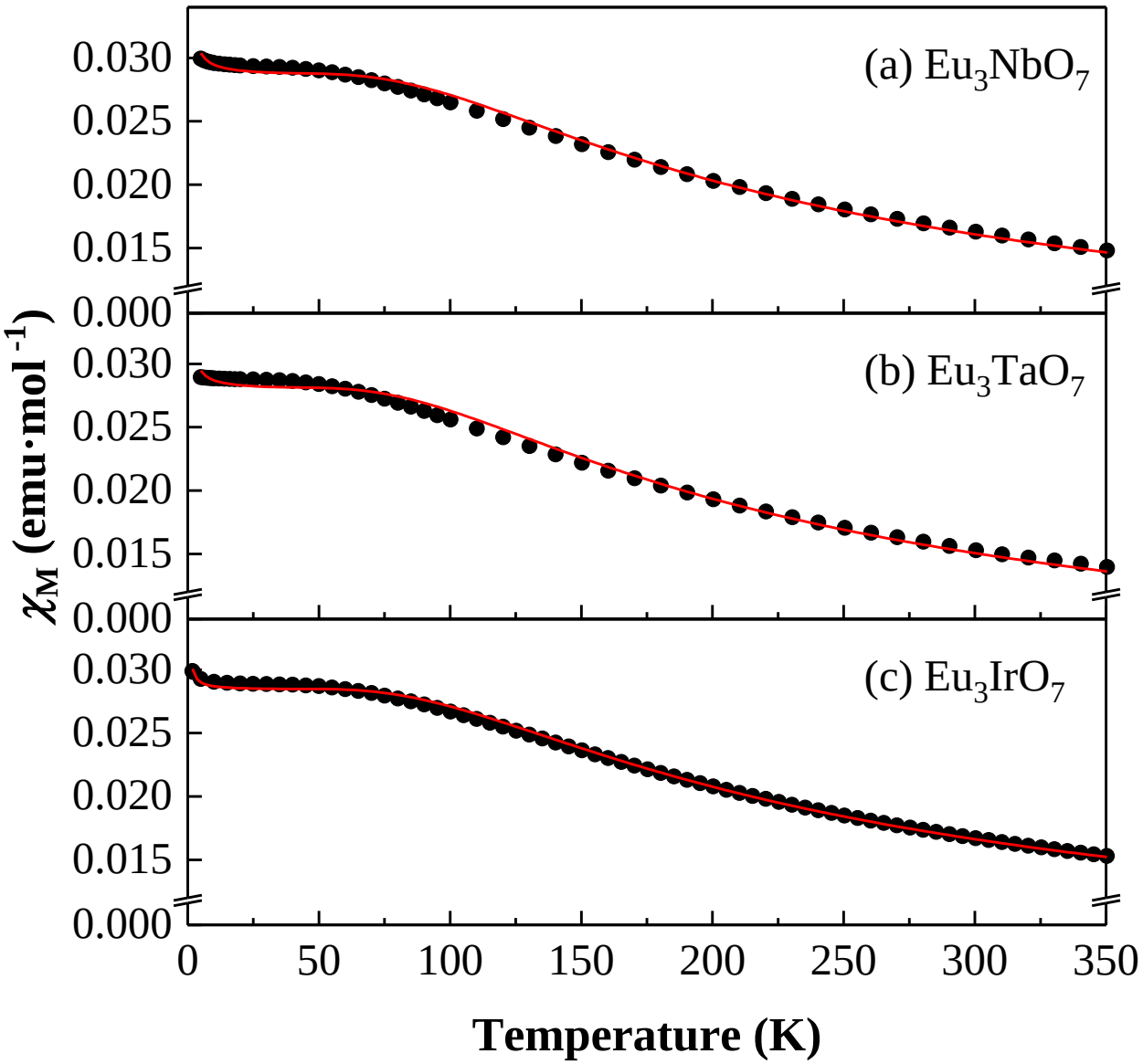
(a) Eu3NbO7
(b) Eu3TaO7
(c) Eu3IrO7
χM (emu·mol-1)
0.030
0.025
0.020
0.015
0.000
0
50
100
150
200
250
300
350
Temperature (K)

Fig.3

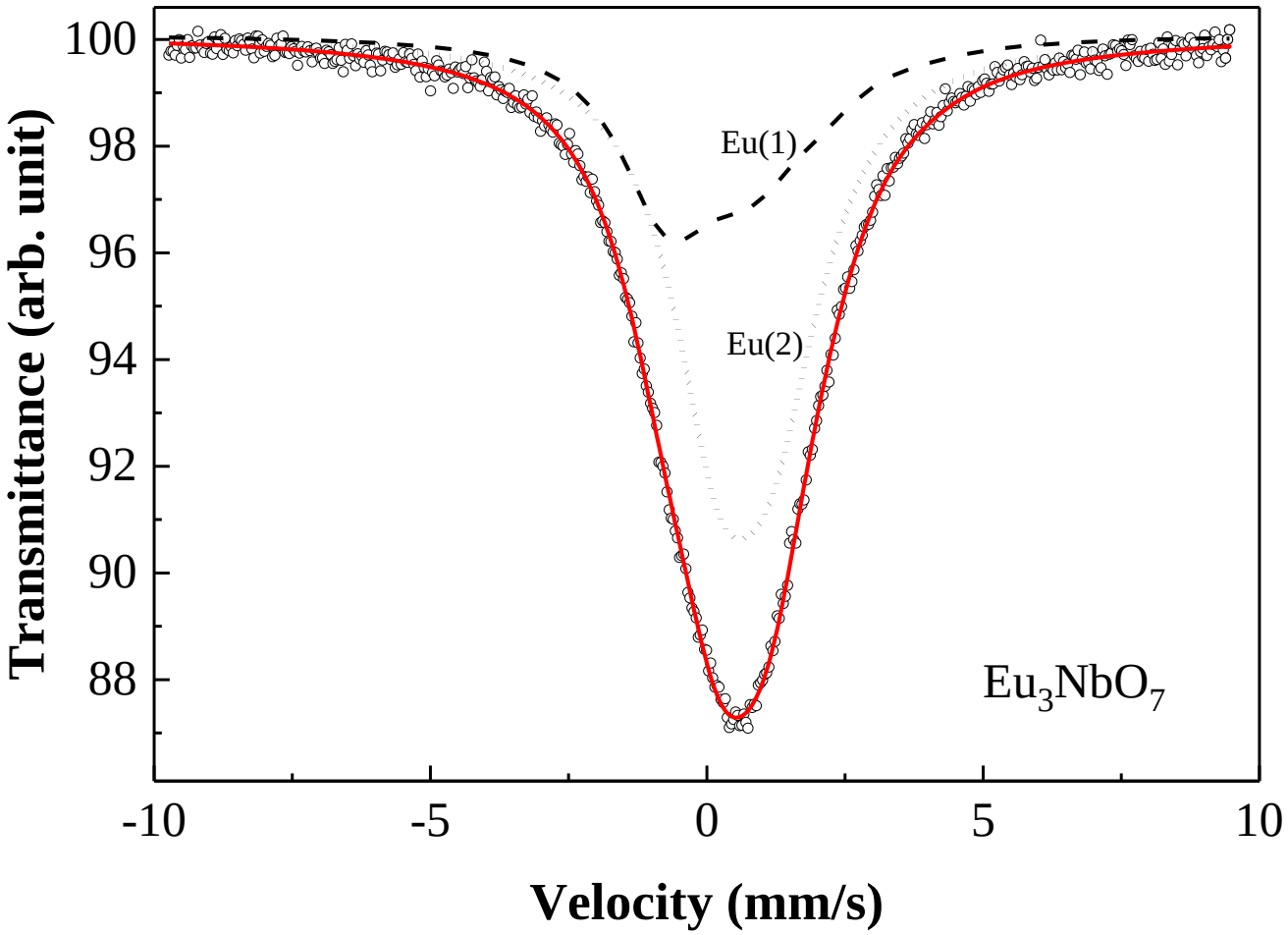
Transmittance (arb. unit)
100
98
96
94
92
90
88
-10
-5
0
5
10
Velocity (mm/s)
Eu(1)
Eu(2)
Eu3NbO7

Fig.4(a)

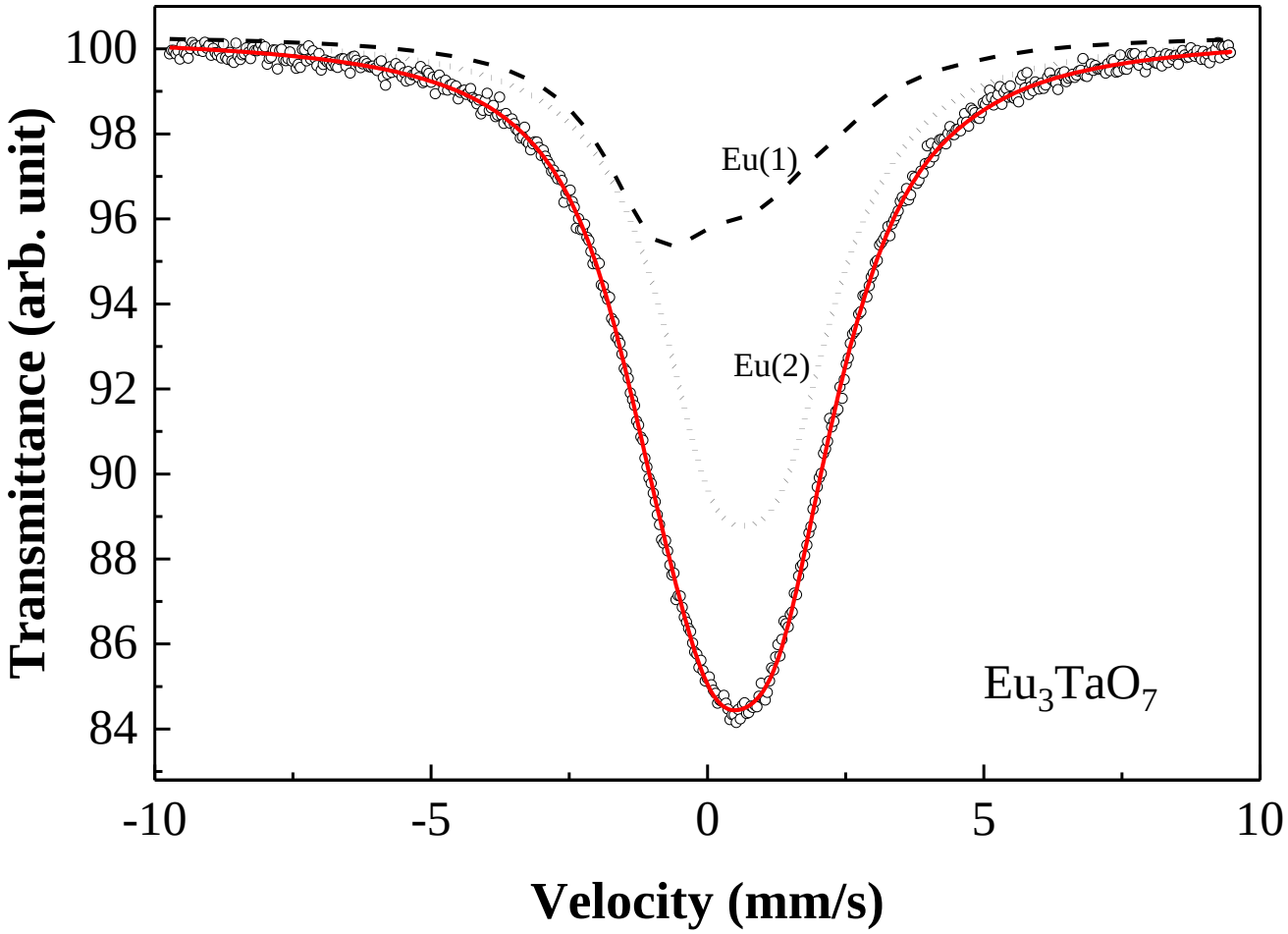
Transmittance (arb. unit)
100
98
96
94
92
90
88
86
84
-10
-5
0
5
10
Velocity (mm/s)
Eu(1)
Eu(2)
Eu3TaO7

Fig.4(b)

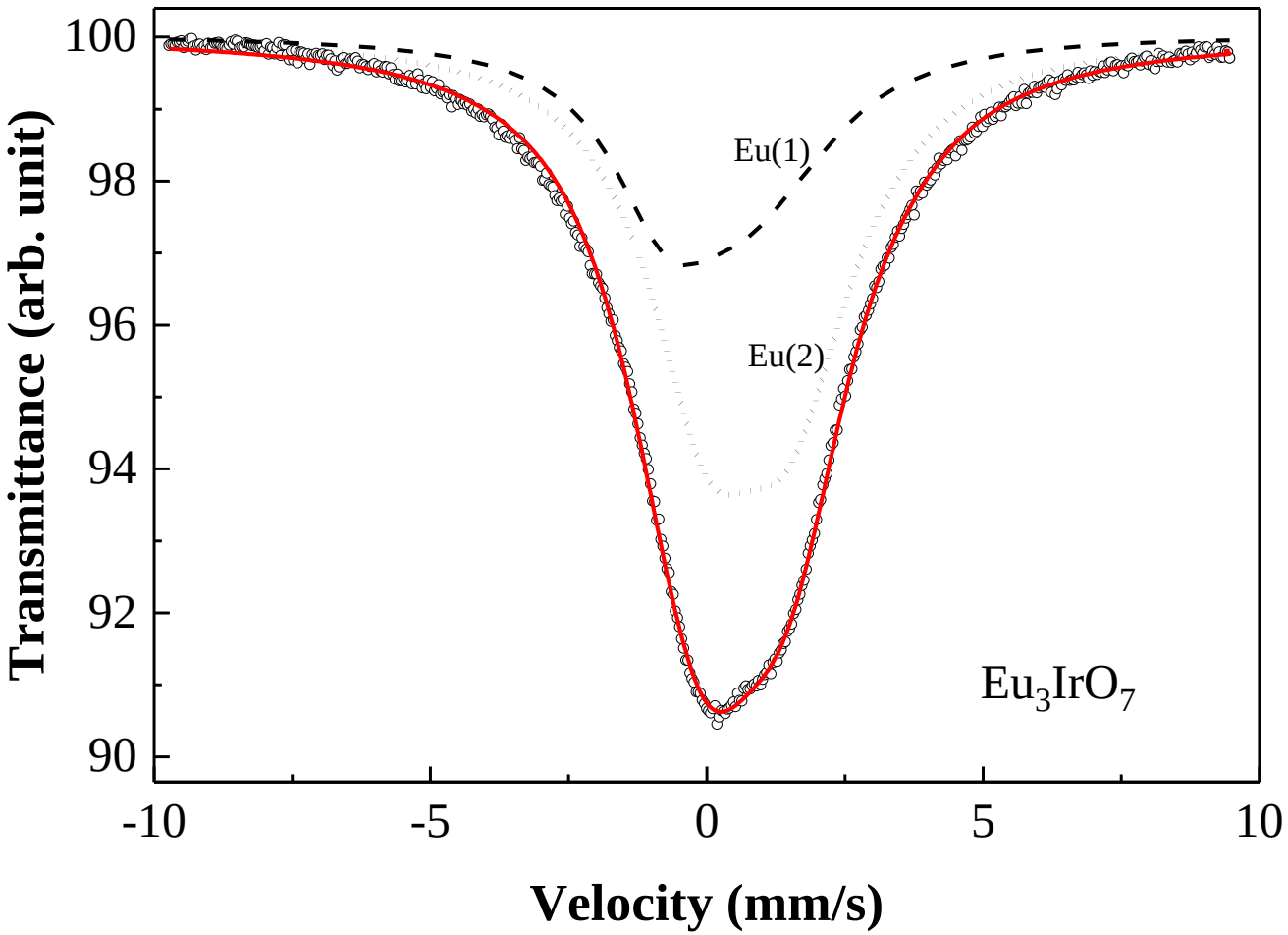
Transmittance (arb. unit)
100
98
96
94
92
90
-10
-5
0
5
10
Velocity (mm/s)
Eu(1)
Eu(2)
Eu3IrO7

Fig.4(c)

Table 1. Structural parameters for Eu_3MO_7 (M = Nb, Ta, Ir).

Eu_3NbO_7

Atom	Site	*x*	*y*	*z*	*B* / Å^2 [a]
Eu(1)	4*b*	0	0.4954(9)	1/4	0.49(3)
Eu(2)	8*c*	0.2338(2)	0.2349(2)	0.0002(1)	0.49
Nb	4*b*	0	0.9992(9)	1/4	0.51(8)
O(1)	8*c*	0.129(4)	0.177(4)	0.273(4)	0.69(7)
O(2)	8*c*	0.116(3)	0.794(4)	0.279(4)	0.69
O(3)	4*a*	0.138(1)	1/2	0	0.69
O(4)	4*a*	0.145(2)	1/2	1/2	0.69
O(5)	4*a*	0.057(3)	0	0	0.69

Note. Space group $C222_1$; a = 10.6480(4) Å, b = 7.5064(3) Å, c = 7.5829(3) Å, V = 606.089(4) Å^3, R_{wp} = 8.91 %, R_I = 2.56 %, and R_e = 6.69 %, where

$$R_{wp} = \left[\sum_i w_i (y_i - f_i(x))^2 / \sum_i w_i y_i^2 \right]^{1/2}, \quad R_I = \sum |I_k(o) - I_k(c)| / \sum I_k(o), \text{ and}$$

$$R_e = \left[(N - P) / \sum_i w_i y_i^2 \right]^{1/2}.$$

a: For the same ions, *B* values were fixed to be equal.

Eu_3TaO_7

Atom	Site	*x*	*y*	*z*	*B* / Å^2 [a]
Eu(1)	4*b*	0	0.4934(9)	1/4	1.15(5)
Eu(2)	8*c*	0.2345(2)	0.2354(2)	0.0000(1)	1.15
Ta	4*b*	0	0.9992(9)	1/4	0.69(7)
O(1)	8*c*	0.139(4)	0.184(4)	0.281(4)	0.7(1)
O(2)	8*c*	0.110(3)	0.782(4)	0.285(4)	0.7
O(3)	4*a*	0.130(1)	1/2	0	0.7
O(4)	4*a*	0.138(2)	1/2	1/2	0.7
O(5)	4*a*	0.065(3)	0	0	0.7

Note. Space group $C222_1$; a = 10.6655(4) Å, b = 7.5163(3) Å, c = 7.5822(3) Å, V = 607.8278(4) Å^3, R_{wp} = 8.06 %, R_I = 1.94 %, and R_e = 6.09 %.

a: For the same ions, *B* values were fixed to be equal.

Eu_3IrO_7

Atom	Site	*x*	*y*	*z*	*B* / Å^2 [a]
Eu(1)	4*a*	0	0	0	0.52(4)
Eu(2)	8*g*	0.225(1)	0.299(2)	1/4	0.52
Ir	4*b*	0	1/2	0	0.30(4)
O(1)	16*h*	0.136(1)	0.309(1)	-0.033(1)	1.2(1)
O(2)	8*g*	0.126(2)	0.024(2)	1/4	1.2
O(3)	4*c*	0	0.411(2)	1/4	1.2

Note. Space group *Cmcm*; a = 10.6807(10) Å, b = 7.39238(6) Å, c = 7.41024(6) Å, V = 585.083(9) Å^3, R_{wp} = 14.35 %, R_I = 3.84 %, and R_e = 10.34 %.

a: For the same ions, *B* values were fixed to be equal.

Table 2. Selected bond lengths (in Å) and bond angles (in degree) for Eu_3MO_7 (M = Nb, Ta, Ir).

Eu_3NbO_7			average
	Eu(1)-O(1) ×2	2.762(11)	
	Eu(1)-O(2) ×2	2.569(8)	
	Eu(1)-O(3) ×2	2.399(6)	2.544
	Eu(1)-O(4) ×2	2.445(8)	
	Eu(2)-O(1)	2.354(9)	
	Eu(2)-O(1)	2.390(8)	
	Eu(2)-O(2)	2.258(10)	
	Eu(2)-O(2)	2.470(10)	2.353
	Eu(2)-O(3)	2.236(10)	
	Eu(2)-O(4)	2.185(9)	
	Eu(2)-O(5)	2.579(9)	
	Nb-O(1) ×2	1.923(8)	
	Nb-O(2) ×2	1.987(10)	1.967
	Nb-O(5) ×2	1.991(8)	
	Nb-O(5)-Nb	144.5(19)	

Eu_3TaO_7			average
	Eu(1)-O(1) ×2	2.768(12)	
	Eu(1)-O(2) ×2	2.480(8)	
	Eu(1)-O(3) ×2	2.349(7)	2.499
	Eu(1)-O(4) ×2	2.400(9)	
	Eu(2)-O(1)	2.224(8)	
	Eu(2)-O(1)	2.393(9)	
	Eu(2)-O(2)	2.352(11)	
	Eu(2)-O(2)	2.540(12)	2.364
	Eu(2)-O(3)	2.280(8)	
	Eu(2)-O(4)	2.232(9)	
	Eu(2)-O(5)	2.530(9)	
	Ta-O(1) ×2	2.045(12)	
	Ta-O(2) ×2	2.028(10)	2.030
	Ta-O(5) ×2	2.018(10)	
	Ta-O(5)-Ta	139.8(20)	

Eu_3IrO_7			average
	Eu(1)-O(1) ×4	2.718(5)	
	Eu(1)-O(2) ×4	2.300(4)	2.509
	Eu(2)-O(1) ×2	2.304(5)	
	Eu(2)-O(1) ×2	2.330(4)	
	Eu(2)-O(2)	2.290(5)	2.343
	Eu(2)-O(2)	2.300(3)	
	Eu(2)-O(3)	2.542(4)	
	Ir-O(1) ×4	2.040(3)	
	Ir-O(3) ×2	1.966(4)	2.016
	Ir-O(3)-Ir	140.9(22)	

Table 3. Isomer shifts, quadruple splitting parameters, and asymmetric parameters for Eu_3MO_7 (M = Nb, Ta, Ir).

		Eu_3NbO_7	Eu_3TaO_7	Eu_3IrO_7
Eu(1)	I.S. (mm/s)	0.19(9)	0.16(8)	0.14(8)
	$eV_{zz}Q_g$ (mm/s)	-7.5(8)	-8.5(8)	-6.7(7)
	η	0.19(7)	0.14(7)	0.28(5)
Eu(2)	I.S. (mm/s)	0.71(5)	0.71(5)	0.79(4)
	$eV_{zz}Q_g$ (mm/s)	-3.9(7)	-4.8(7)	-5.9(3)
	η	0.59(8)	0.87(9)	0.81(8)